J. Fluid Mech. (1980), *vol.* 96, *part* 4, *pp.* 735–756
Printed in Great Britain

Domains and boundaries of non-stationary oblique shock-wave reflexions. 2. Monatomic gas

By G. BEN-DOR† AND I. I. GLASS
Institute for Aerospace Studies, University of Toronto, Ontario, Canada M3H 5T6

(Received 3 January 1979)

Interferometric data were obtained in the 10 cm × 18 cm hypervelocity shock tube of oblique shock-wave reflexions in argon at initial temperatures and pressures of nearly 300 °K and 15 Torr. The shock Mach number range covered was $2 \leqslant M_s \leqslant 8$ over a series of wedge angles $2^\circ \leqslant \theta_w \leqslant 60^\circ$. Dual-wavelength laser interferograms were obtained by using a 23 cm diameter field of view Mach–Zehnder interferometer. In addition to our numerous results, the available data for argon and helium obtained over the last two decades were also utilized. It is shown analytically and experimentally that in non-stationary flows six domains exist in the (M_s, θ_w) plane where regular reflexion (RR), single-Mach reflexion (SMR), complex-Mach reflexion (CMR) and double-Mach reflexion (DMR) can occur. The transition boundaries between these regions were all established analytically. The experimental results from different sources substantiate the present analysis, and areas of disagreement which existed in the literature are now clarified and resolved. It is shown that real-gas effects have a significant influence on the size of the regions and their boundaries. In addition, isopycnics (constant density lines) are given for the four types of reflexion, as well as the density distribution along the wedge surface. This data should provide a solid base for computational fluid dynamicists in comparing numerical techniques with actual experimental results.

1. Introduction

When a planar moving shock wave encounters a sharp compressive corner in a shock tube, two processes take place simultaneously. The incident shock wave is reflected by the wedge surface, whereas the induced non-stationary flow behind it is deflected by the wedge corner. In the following, the first process will be referred to as shock-wave reflexion, the second as flow deflexion, and the overall phenomena as shock-wave diffraction.

Shock-wave diffractions depend on three factors: (1) Mach number M_s of the incident shock wave; (2) corner wedge angle θ_w; (3) initial thermodynamic state of the gas, i.e. temperature T_0 and pressure P_0 (for a perfect gas, these are not required).

Four different types of reflexion have been observed in shock-tube experiments. They are regular reflexion (RR), single-Mach (SMR), complex-Mach (CMR) and double-Mach reflexions (DMR). An interferogram of each reflexion as well as explanatory sketches are shown in figure 1 (plate 1). The phenomena of RR and SMR were

† Present address: Department of Mechanical Engineering, Ben-Gurion University of the Neger, Beer-Sheva, Israel.

0022–1120/80/4380–8310 $02.00

first discovered by E. Mach (1878), CMR by Smith (1945) and DMR by White (1951) The reflexion and diffraction phenomena have been investigated quite intensively in the last three decades by many researchers. Unfortunately, however, most of these analytical and experimental investigations were done on diatomic gases such as air, oxygen and nitrogen (von Neumann 1943, 1945; Seeger & Polacheck 1943; Smith 1945; Taub 1947; Bleakney & Taub 1949; Fletcher 1951; White 1951; Jones, Martin & Thornhill 1951; Kawamura & Saito 1956; Molder 1960, 1979; Henderson 1964; Gvozdeva *et al.* 1969; Law & Glass 1971; Henderson & Lozzi 1975; Bazhenova, Fokeev & Gvozdeva 1976; Auld & Bird 1976; Ben-Dor & Glass 1978, 1979; Ben-Dor 1978*a*, *b*). Very few researchers investigated the phenomena in monatomic gases (Gvozdeva *et al.* 1969; Bazhenova *et al.* 1976; Molder 1979; Hornung, private communication; Hornung, Oertel & Sandeman 1979; Ben-Dor 1978*a*, *b*). Consequently, unlike a diatomic gas where the domains of different types of reflexion and their transition boundaries were established analytically and experimentally in final and complete form by Ben-Dor & Glass (1979) for both perfect and imperfect diatomic gases, a lack of analytical and experimental information both for perfect and imperfect monatomic gases exists in the literature. We have therefore tried to rectify this situation by establishing the domains and their boundaries analytically and experimentally in monatomic gases as well.

2. Analysis

As mentioned above the shock-wave reflexion process interacts with the flow deflexion process to yield the overall shock-wave diffraction phenomenon. In the following, each of these processes is discussed in detail.

Shock-wave reflexion

Ben-Dor & Glass (1979) and Ben-Dor (1978*a*) have recently shown the significance of real-gas effects on shifting the transition lines between the domains of different reflexions. The formation and termination criteria of RR, SMR, CMR and DMR are all discussed in detail by Ben-Dor (1978*a*); consequently, only a brief discussion follows.

The criterion for the termination of RR makes use of the boundary condition that the flow downstream of the reflexion point must be parallel to the wall, i.e. $\theta_1 + \theta_2 = 0$ (θ_1 and θ_2 are the flow deflexions through the incident and reflected shock waves, respectively). When this is violated [i.e. θ_w decreases to a point where it forces θ_1 to exceed in magnitude the maximum deflexion value θ_{2m} of the flow in state (1), figure 1(*a*)], RR terminates. Therefore the termination criterion is

$$\theta_1 + \theta_{2m} = 0. \tag{1}$$

This criterion was first established by von Neumann (1943). Henderson & Lozzi (1975) advanced another criterion for the termination of RR. However, Hornung (private communication), Hornung *et al.* (1979) and Ben-Dor & Glass (1979) have recently shown that the Henderson & Lozzi criterion is not applicable to non-stationary flows. Hornung and Hornung *et al.* (1979) advanced another criterion for the termination of RR that differs only slightly from the 'detachment criterion' described

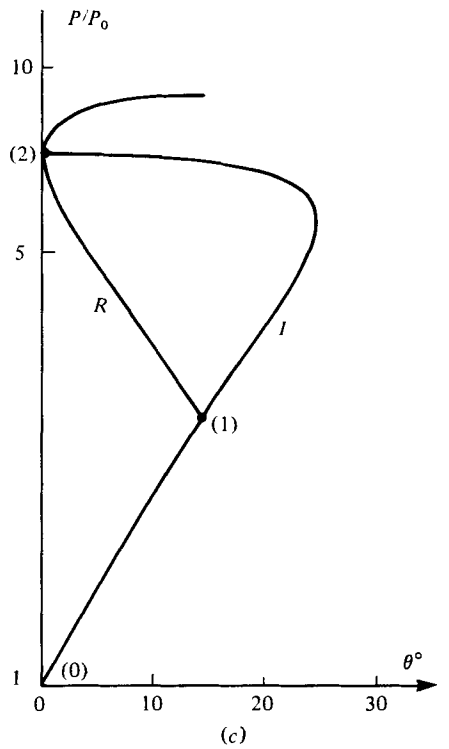

FIGURE 2. I and R polar combination for change-over Mach number M_{0c} in argon. $M_{0c} = 2{\cdot}453$, $M_s = 1{\cdot}540$, $\theta_w = 51{\cdot}13°$.

by (1). They advanced the suggestion that RR terminates when the flow behind the reflected shock wave becomes sonic with respect to the reflexion point, i.e.

$$\theta_1 + \theta_{2s} = 0. \tag{1a}$$

Practically, however, the difference between (1) and (1a) is too small to distinguish between them and hence, in the following, only (1) is considered.

In the (P, θ) plane (pressure-deflexion shock polars), the detachment criterion corresponds to the case where the R polar becomes tangent to the P axis. It is important to mention that Kawamura & Saito (1956) were the first to notice that the point of tangency between the R polar and the P axis can be outside or inside the I polar, depending on whether the value of M_0 ($M_0 = M_s \sec\theta_w$) is greater or less than a certain change-over value M_{0c}. Unlike the case of a diatomic gas for which different values of M_{0c} are reported by various investigators (Kawamura & Saito 1956; Henderson & Lozzi 1975; Molder 1979; Ben-Dor & Glass 1978), only one value is reported for a perfect monatomic gas by Molder (1979) who calculated $M_{0c} = 2{\cdot}470$. The value calculated by us for perfect and imperfect argon is $M_{0c} = 2{\cdot}453$ ($M_s = 1{\cdot}540$ and $\theta_w = 51{\cdot}13°$). The shock-polar combination for this condition is shown in figure 2.

When RR terminates three different types of reflexion, SMR, CMR and DMR, can occur depending on the Mach number of the flow behind the reflected shock wave R. As long as the flow behind R in state 2 is subsonic with respect to the triple point T, i.e. $M_{2T} < 1$, SMR (figure 1b) occurs. When this flow becomes supersonic with respect

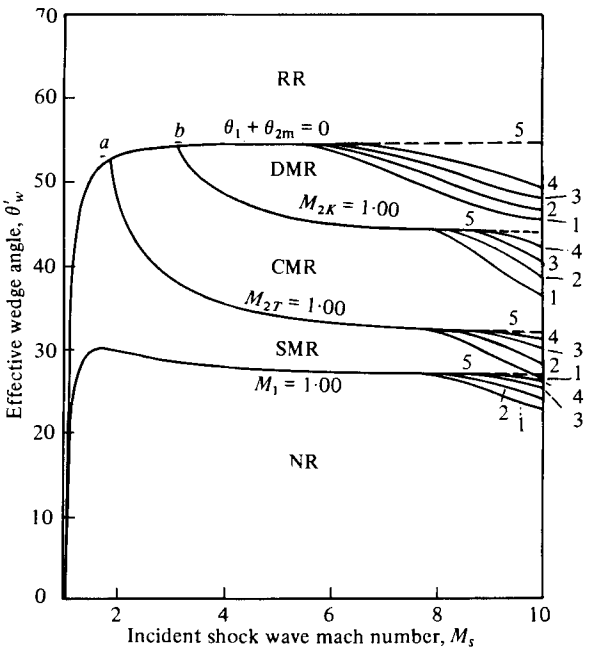

FIGURE 3. Regions of different oblique shock-wave reflexions in (M_s, θ'_w) plane. Lines (1) to (4) are for imperfect argon with P_0 = 1, 10, 100 and 1000 Torr, respectively, and T_0 = 300 °K. Line (5) is for a perfect monatomic gas $\gamma = \frac{5}{3}$.

to T, SMR terminates and a kink K develops in R resulting in a CMR (figure 1*c*). Consequently, the SMR $\rightleftarrows$ CMR transition criterion is

$$M_{2T} = 1. \tag{2}$$

CMR terminates when the flow behind R becomes supersonic with respect to the kink K; thus the CMR $\rightleftarrows$ DMR transition criterion is

$$M_{2K} = 1. \tag{3}$$

The non-stationary shock-wave-reflexion domains in the (M_s, θ'_w) plane for perfect and imperfect argon are shown in figure 3. In addition to the above-mentioned four types of reflexion domains, there is also a domain of no reflexion (NR). It is shown subsequently, however, that this domain disappears when the vertical axis is transformed from the effective wedge angle θ'_w to the actual wedge angle θ_w. (Note that $\theta'_w = \theta_w + \chi$ and χ is the triple-point trajectory angle.) The dashed boundary lines are for a perfect monatomic gas while the solid lines are for argon in ionization equilibrium with four different initial pressures (P_0 = 1, 10, 100 and 1000 Torr) and a constant initial temperature (T_0 = 300 °K). The significance of real-gas effects in shifting the boundary lines can be clearly seen in figure 3. Note that the sharp boundary lines which exist for a perfect gas between the domains of different types of reflexion are replaced by a multiplicity of lines depending on the initial pressure (when the temperature is fixed). For example, one should expect a SMR for M_s = 10 and θ'_w = 30° when $P_0 > 100$ Torr and a CMR when $P_0 < 100$ Torr.

It is worthwhile mentioning that all the lines shown in figure 3 were obtained by

solving the oblique shock-wave equations that describe a RR or a three-shock confluence of the first triple point of SMR, CMR and DMR. These equations were solved with and without real-gas effects. To the best of our knowledge, this is probably the first time that these equations were solved and the results are presented for perfect and imperfect monatomic gases (for details see Ben-Dor 1978*a*). If the incident shock-wave Mach number is fixed while varying the effective wedge angle θ'_w (or actual wedge angle θ_w) different domains of reflexion are encountered. The different sequences of events are: $1{\cdot}00 < M_s < 1{\cdot}85$, RR → SMR (see point *a*); $1{\cdot}85 < M_s < 3{\cdot}17$, RR → CMR → SMR (see point *b*); for $M_s > 3{\cdot}17$, RR → DMR → CMR → SMR. With a proper choice of θ'_w (or θ_w) RR and SMR can occur for any incident shock-wave Mach number M_s, while the other reflexions are limited to defined values of M_s e.g.; CMR can occur only for $M_s > 1{\cdot}85$ (see point *a*) and DMR for $M_s > 3{\cdot}17$ (see point *b*).

Since $M_0 = M_s \sec\theta'_w$ (where $\theta'_w = \theta_w + \chi$ and χ is the triple-point trajectory angle) and $\phi_0 = 90° - \theta'_w$, one might conclude that the domains of different types of reflexion shown in figure 3 are also valid for steady flows. However, besides the fact that the termination criterion for RR in steady flows is different from that of non-stationary flows for $M_0 > M_{0c}$ (Henderson & Lozzi 1975; Hornung, private communication; Hornung *et al.* 1979), CMR and DMR cannot occur in steady flows (Ben-Dor 1978*a*). Consequently, only two reflexion domains are possible, RR and SMR where the flow behind the reflected shock wave can be either subsonic or supersonic.

The vertical axis θ'_w of figure 3 equals $\theta_w + \chi$ in the domains of SMR, CMR and DMR and θ_w in the domain of RR where $\chi = 0$ (χ is the triple-point trajectory angle, see figure 1). Therefore, in order to obtain the domains of different reflexion processes in a more physical plane, i.e. the (M_s, θ_w) plane, χ should be subtracted from the boundary lines of figure 3. Law & Glass (1971) developed a graphical method for predicting χ. An analytical version of their graphical method which was found to be in better agreement with experiments was later developed by Ben-Dor & Glass (1979). The method of Law & Glass (1971) assumes a straight Mach stem normal to the wedge; consequently the value of χ can be found from the simple geometrical relation

$$\chi = 90° - \phi_3, \tag{4}$$

where ϕ_3, the angle of incidence between the Mach stem and the oncoming relative flow, is found by solving the oblique shock-wave equations that describe the triple point (see Ben-Dor 1978*a* for details). Since this method fails to predict the value of χ for small wedge angles, an alternative method for very small wedge angles is suggested in the following. This method is based on the experimental fact that at small wedge angles a SMR occurs even though the flow behind the incident shock wave is subsonic with respect to the reflexion point P. Thus the triple-point trajectory angle plays a significant role (at very small wedge angles) when it makes the effective wedge angle $\theta'_w = \theta_w + \chi$ large enough so that the flow behind the incident shock wave will always be supersonic ($M_1 > 1$) with respect to the triple point. Consequently, a relation of the form $\theta'_w|_{M_1=1} = \theta'_w(M_s, P_0, T_0)$, for which the flow behind the incident shock wave is exactly sonic, can be found easily (see line $M_1 = 1$ for $T_0 = 300$ °K and $P_0 = 1$, 10, 100 and 1000 Torr, respectively, in figure 3). Once this relation is derived. χ can be calculated from

$$\chi = \theta'_w|_{M_1=1} - \theta_w. \tag{5}$$

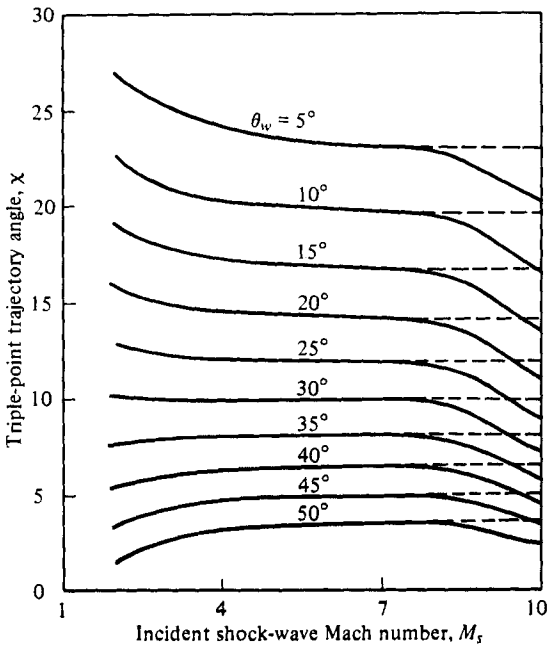

FIGURE 4. Variation of χ with M_s for a given θ_w. Solid lines, imperfect argon, $P_0 = 15$ Torr, $T_0 = 300$ °K; dashed lines, perfect monatomic gas, $\gamma = \frac{5}{3}$.

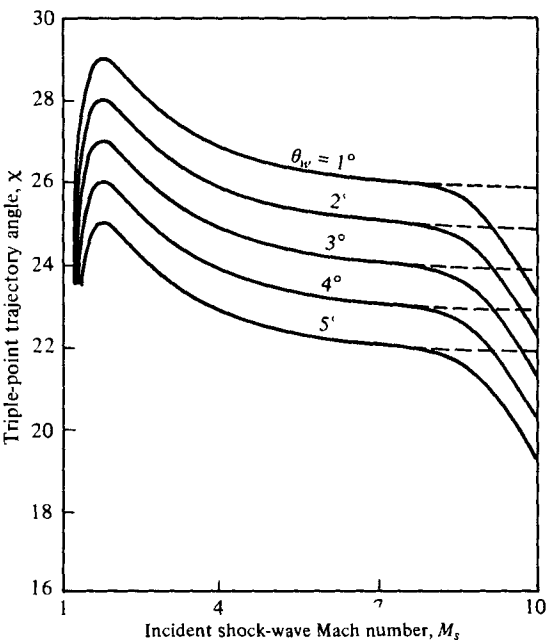

FIGURE 5. Variation of χ with M_s for a given θ_w. Solid lines, imperfect argon, $P_0 = 15$ Torr, $T_0 = 300$ °K; dashed lines, perfect monatomic gas, $\gamma = \frac{5}{3}$.

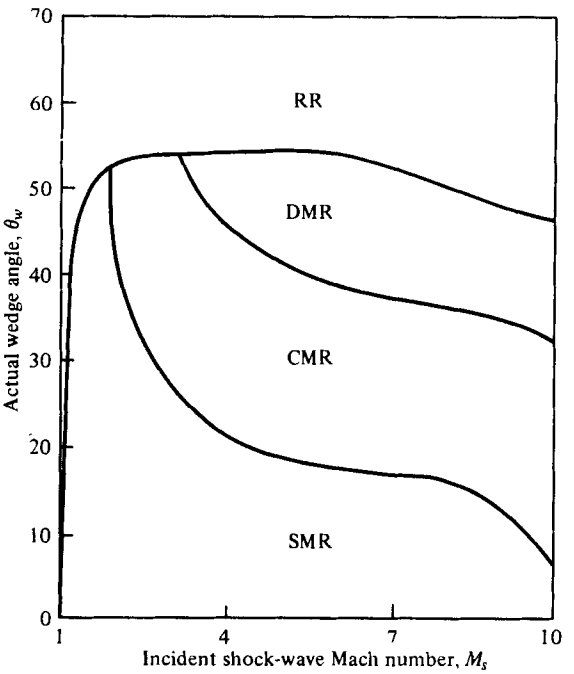

FIGURE 6. Regions of different oblique shock-wave reflexions in (M_s, θ_w) plane. All boundary lines are for imperfect argon with $P_0 = 15$ Torr and $T_0 = 300$ °K.

The dependence of χ on M_s and θ_w using our analytical version of the method developed by Law & Glass (1971) [equation (4)] and the present method for small wedge angles [equation (5)] are shown in figures 4 and 5, respectively. The solid lines are for imperfect argon with $P_0 = 15$ Torr and $T_0 = 300$ °K and the dashed lines are for a perfect monatomic gas. It can be seen that the imperfect-gas lines (solid) start to diverge from the perfect-gas lines (dashed) at $M_s \sim 7$ and hence the perfect-gas model is adequate in the range $1 \leqslant M_s \leqslant 7$. Note that the perfect-gas lines level out as M_s increases, resulting in a situation in which χ is independent of M_s, i.e. $\chi = \chi(\theta_w)$. In reality, however, ionization starts at $M_s > 7$ and consequently the dependence of χ upon M_s increases. It is worth mentioning that although figure 5 is based only on the experimental fact that SMR occur even for very low wedge angles, it resembles the properties of figure 4 (the curves for $\theta_w < 15°$), which is based on the reasonable physical assumption of a straight Mach stem. In both figures 4 and 5, χ is a decreasing function of M_s and θ_w. However for an imperfect gas the dependence of χ upon M_s is significant as M_s increases due to ionization, while the perfect-gas lines (dashed) level out, resulting in a situation in which χ is independent of M_s.

The non-stationary shock-wave reflexion phenomenon in the (M_s, θ_w) plane, i.e. figure 3 with χ subtracted, is shown in figure 6. Only lines corresponding to $P_0 = 15$ Torr and $T_0 = 300$ °K are drawn. Note that the NR domain has disappeared. Therefore an incident shock wave will always reflect when it collides with a compression corner in a shock tube.

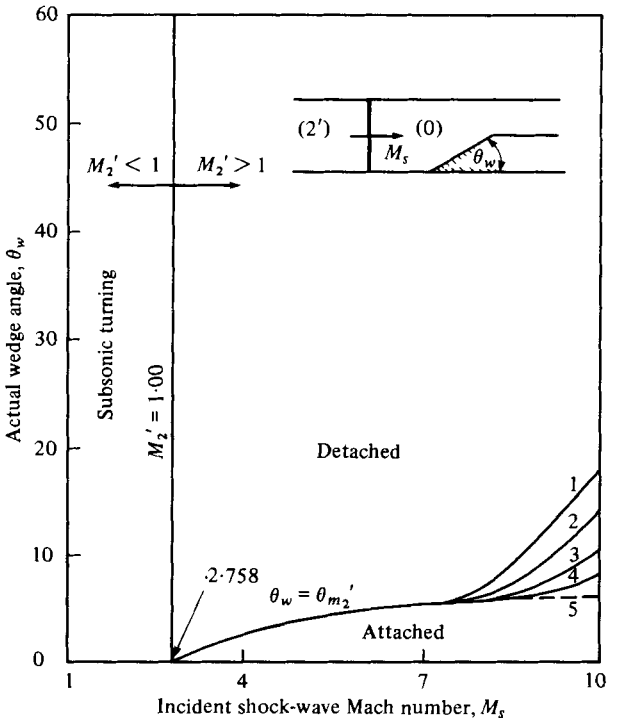

FIGURE 7. Deflexion processes of shock-induced quasi-steady flow (2') as a function of M_s and θ_w. Lines (1) to (4) are for imperfect argon, $T_0 = 300$ °K, and $P_0 = 1$, 10, 100 and 1000 Torr, respectively. Line (5) is for a perfect monatomic gas, $\gamma = \frac{5}{3}$.

Induced flow deflexion

Consider a planar shock wave propagating in a shock tube (figure 7) and denote the induced flow behind it as (2'). For any given set of initial conditions (P_0 and T_0) and incident shock Mach number M_s, the induced flow Mach number $M_{2'}$ as well as its pressure $P_{2'}$ and temperature $T_{2'}$ can be calculated. Consequently, the corresponding sonic deflexion angle $\theta_{s2'}$ and the angle of maximum deflexion $\theta_{m2'}$ for this induced flow can be determined. Thus the (M_s, θ_w) plane is now divided into two main regions. One region corresponds to $M_{2'} < 1$ where the induced flow is subsonic and can turn the corner subsonically. The other region corresponds to $M_{2'} > 1$, where the flow is supersonic. The latter region can be further divided into three sub-regions of different flow deflexion processes: $0 < \theta_w < \theta_{s2'}$ for deflexion through a straight and attached shock wave, $\theta_{s2'} < \theta_w < \theta_{m2'}$ for deflexion through a curved and attached shock wave, and $\theta_w > \theta_{m2'}$ where the deflexion is through a curved and detached shock wave. For practical purposes, since the maximum separation between $\theta_{s2'}$ and $\theta_{m2'}$ is usually very small (less than 1°), only two regions, $0 < \theta_w < \theta_{m2'}$ where the shock wave is attached and $\theta_w > \theta_{m2'}$ where it is detached, need be considered.

The domains of the different types of flow-deflexion processes for argon in the (M_s, θ_w) plane are shown in figure 7. The dashed line is for a perfect monatomic gas ($\gamma = \frac{5}{3}$) and the solid lines are for imperfect argon with different initial pressures ($P_0 = 1$, 10, 100 and 1000 Torr) and a constant initial temperature ($T_0 = 300$ °K).

It can be seen again that the imperfect-gas boundary lines start to diverge from the

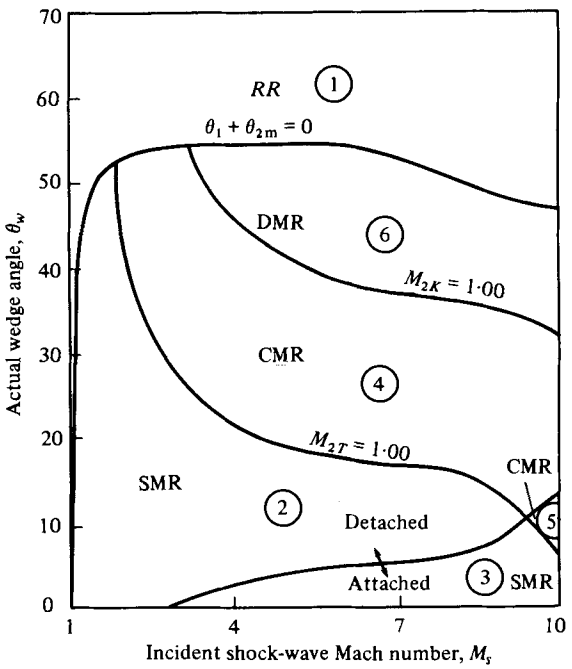

FIGURE 8. Six domains and their transition boundaries of non-stationary shock-wave diffraction in (M_s, θ_w) plane. Imperfect argon, $P_0 = 15$ Torr, $T_0 = 300$ °K (see table 1).

perfect-gas line (dashed) at relatively high values of M_s (i.e. $M_s \approx 7{\cdot}3$). Consequently, the perfect-gas model is adequate in the range $M_s < 7{\cdot}3$. Note that the line $M_{2'} = 1{\cdot}00$ corresponds to $M_s = 2{\cdot}758$ for both perfect and imperfect gases. The dependence of the deflexion process on real-gas effects (at high values of M_s) is again clearly seen (figure 7). For $M_s = 10$ and $\theta_w = 10°$ the flow will negotiate the corner through an attached shock wave if $P_0 \leqslant 10$ Torr or a detached shock wave if $P_0 \geqslant 100$ Torr.

Shock-wave diffraction

The overall shock-wave diffraction phenomenon is obtained by superimposing the shock-wave reflexion process (figure 6) and the flow-deflexion process (figure 7). It has been shown by Ben-Dor & Glass (1979) that owing to the interaction of the shock-wave reflexion and induced flow-deflexion processes, the subsonic turning region shown in figure 7 cannot materialize. Consequently, since four shock-wave reflexions and two flow deflexions are possible, a maximum of eight different types of shock-wave diffraction might hypothetically be obtained. Figures 6 and 7 were superimposed to obtain figure 8. For clarity, only lines corresponding to imperfect argon at $P_0 = 15$ Torr and $T_0 = 300$ °K are reproduced. In the range $1 \leqslant M_s \leqslant 10$ only six diffractions out of the maximum eight are possible. The two unobtainable diffractions are a RR and a DMR with an attached shock wave at the corner. However, if the two lines $\theta_1 + \theta_{2m} = 0$ and $M_{2K} = 1{\cdot}00$ and the attached/detached line ($\theta_w = \theta_{m2'}$) are extrapolated beyod $M_s = 10$, they might intersect, making it possible to obtain the two missing diffractions. Note that this could also be obtained by reducing the initial pressure. The six different shock-wave diffractions in the range $1 \leqslant M_s \leqslant 10$ (figure 8)

Region no.	Shock diffraction: Shock reflexion	Shock diffraction: Flow deflexion
1	RR	Detached
2	SMR	Detached
3	SMR	Attached
4	CMR	Detached
5	CMR	Attached
6	DMR	Detached

TABLE 1. Diffraction regions in argon (see figure 8)

are RR with a detached shock wave (region 1), SMR with a detached or an attached shock wave (regions 2 and 3, respectively), CMR with a detached or an attached shock wave (regions 4 and 5, respectively), and DMR with a detached shock wave (region 6). The six different types of diffractions are listed in table 1.

3. Verification of diffraction domains and boundaries

In order to verify the above-discussed analyses of the shock-wave reflexion and diffraction phenomena, 48 successful experiments were done in the 10 cm × 18 cm UTIAS hypervelocity shock tube. A 23 cm diameter Mach–Zehnder interferometer was used for recording the non-stationary process. The light source consisted of a giant-pulse ruby laser. Simultaneous dual-frequency interferograms were taken at wavelengths of 6943 Å and 3471·5 Å. Wedges with $\theta_w = 2°$, 10°, 20°, 30°, 40°, 50° and 60° ($\pm 1/30°$) were used. Each wedge was fastened to the lower wall of the test section of the shock tube. The clearance between the wedge and the shock tube side walls or windows was 0·025 mm. Although this arrangement tends to introduce boundary-layer interaction at the wedge corner, it was adopted owing to the simplicity in design and the rigid fastening which is especially important on impact with a strong shock wave. For each wedge about seven experiments were made at the following nominal incident shock wave Mach numbers: $M_s = 2{\cdot}0$, 2·9, 4·4, 5·2, 6·0, 7·0, and 8·0. Over this range the Mach number varied by about 0·1. The accuracy in measuring the shock wave Mach number was $E(M_s) = 0{\cdot}0011M_s^2 + 0{\cdot}01018M_s$, which gives a relative error of 1·25 % at $M_s = 2{\cdot}0$ [$E(M_s) = 0{\cdot}025$] and 1·90 % at $M_s = 8{\cdot}0$ [$E(M_s) = 0{\cdot}152$]. We did not go beyond $M_s = 8{\cdot}0$, as in similar previously conducted experiments in the same facility (Law & Glass 1971) the high-quality optical windows of the test section were burned.

The initial pressure P_0 was measured with an oil manometer just after admitting the test gas, to an accuracy of $E(P_0) = [1{\cdot}398 \times 10^{-5}H + 0{\cdot}0786]$ Torr, where H is the height difference in the manometer in millimetres. Since 15 Torr corresponds to $H = 194$ mm, an error of 0·54 % [$E(P_0) = 0{\cdot}081$] is associated with this measurement. The pressure P_0 was kept at 15 Torr for the runs with $M_s = 4{\cdot}4$, 5·2, 6·0 and 7·0, 9·8 Torr for $M_s = 8{\cdot}0$, and 50 Torr for $M_s = 2{\cdot}0$. The driving gases used to obtain the shock-wave Mach numbers with the given initial pressures were He, H_2 and CO_2, respectively. The initial driver and test gas temperatures T_0 were usually in the range 295–299 °K, and measured to an accuracy of 0·1 °K.

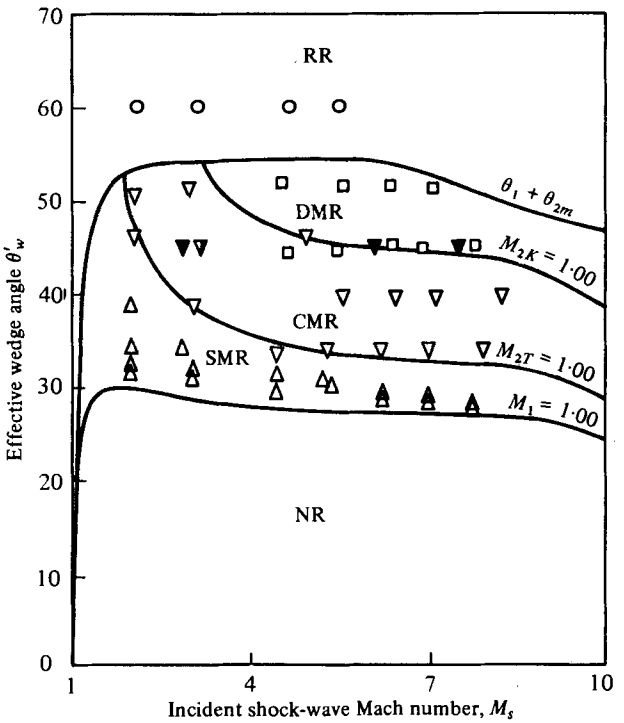

FIGURE 9. Experimental verification of oblique shock-wave reflexion analysis (pseudo-stationary frame of reference). Imperfect argon, $P_0 = 15$ Torr, $T_0 = 300$ °K. Present data: □, DMR; ▽, CMR; △, SMR; ○, RR. Previously obtained data: ▼, CMR in argon (Law & Glass 1971); ▼, CMR in helium (Law 1970). Note the term reflexion is used since the results are plotted in the pseudo-stationary (M_s, θ'_w) plane.

In addition to our results (see Ben-Dor 1978*b* for a detailed listing of the initial conditions and the corresponding interferograms), the experimental data of Law & Glass (1971) in argon and helium, and Gvozdeva *et al.* (1969) and Bazhenova *et al.* (1976) in argon were also used.

It is worth mentioning again that in the present analysis two different phenomena, the shock-wave reflexion process at the wedge surface (figure 3), and the induced flow-deflexion process (figure 7) over the wedge corner were treated independently. The shock-wave reflexion process was then transformed from the (M_s, θ'_w) plane (figure 3) to the actual (M_s, θ_w) plane (figure 6), by subtracting from θ'_w the appropriate value of the triple-point trajectory angle χ (figures 4, 5), in order to superimpose these two processes (figures 6, 7), and then finally obtain the overall shock-wave diffraction process (figure 8).

In the following, the above-mentioned analyses for the non-stationary reflexion of shock waves in the (M_s, θ'_w) and (M_s, θ_w) planes, the methods of predicting χ and the non-stationary diffraction of shock waves in the (M_s, θ_w) plane are compared with experiments. The present experimental results (Ben-Dor 1978*b*) in argon as well as some data from Law & Glass (1971) in argon and from Law (1970) in helium are all shown in figure 9 (a reproduction of figure 3 for $P_0 = 15$ Torr). Some experiments that are reported by Law & Glass as CMR lie inside the DMR domain ($M_s = 6{\cdot}10$ and $7{\cdot}66$,

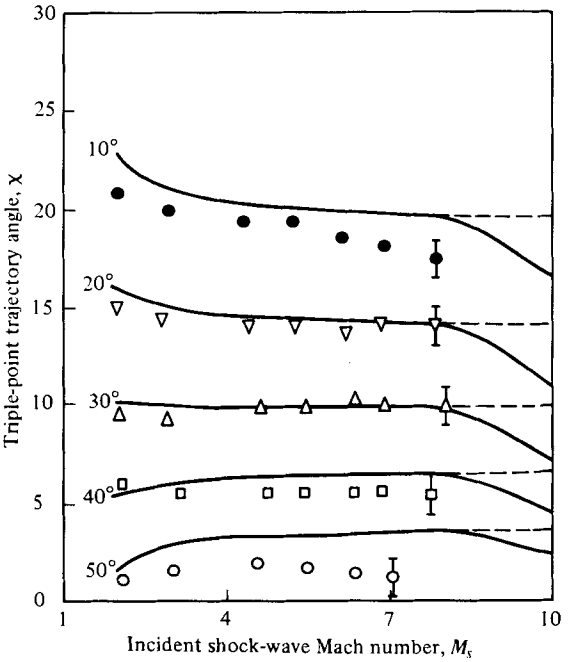

FIGURE 10. Verification of χ *vs.* M_s with θ_w and comparison with experiments. Solid lines, imperfect argon, $P_0 = 15$ Torr, $T_0 = 300$ °K; dashed lines, perfect monatomic gas, $\gamma = \frac{5}{3}$. All data points are from the present study. θ_w: ○, 50°; □, 40°; △, 30°; ▽, 20°; ●, 10°.

$\theta_w \sim 45°$). These experiments, however, are surrounded by experimental points from the present study that showed a DMR. It is possible that the initial direction of the fringes chosen by Law & Glass (different from ours) was such that the R shock wave (figure 1*d*) of a DMR could not be seen clearly. Note that Bazhenova *et al.* (1976) also reported DMR in argon in a region where Law & Glass reported CMR configurations.

Out of all the present experiments, only one ($M_s \sim 4$, $\theta'_w \sim 45°$) that corresponds to a DMR lies outside its predicted region, in the CMR domain. This we believe is due to the fact that in calculating the CMR/DMR boundary line ($M_{2K} = 1{\cdot}00$) we have used a relation that was found to be in good agreement with experiments only in the range $\theta_w < 40°$. For the range $\theta_w > 40°$ the agreement became progressively worse (see Ben-Dor 1978*a* for details). It is worth mentioning that, apart from this slight disagreement, all the other experimental points lie inside their predicted domains.

The present data (Ben-Dor 1978*b*) for $\theta_w = 10°$, 20°, 30°, 40°, 50° and 60° are shown in figure 10 (a reproduction of figure 4) in order to test the present analytical method (based on Law & Glass 1971, graphical method) for predicting χ. Very good agreement can be seen with the wedge angles of 20°, 30° and 40° while for 10° and 50° the actual value of χ is smaller than the predicted one by more than 1° (the error bar). For these two wedge angles, the agreement is fairly good for small values of M_s ($M_s < 3$ for $\theta_w = 50°$ and $M_s < 5$ for $\theta_w = 10°$) and becomes progressively worse as M_s increases.

The data points for $\theta_w = 2°$ are shown in figure 11 (a reproduction of figure 5 for $\theta_w = 2°$). The agreement between theory and experiment is fairly good for low and

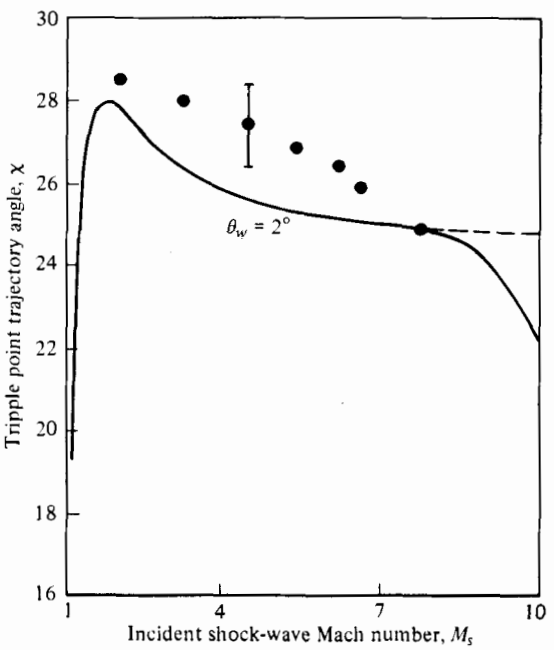

FIGURE 11. Variation of χ *vs.* M_s for small θ_w and comparison with experiments. Solid line, imperfect argon, $P_0 = 15$ Torr, $T_0 = 300$ °K; dashed line, perfect monatomic gas $\gamma = \frac{5}{3}$. All data points are from the present study.

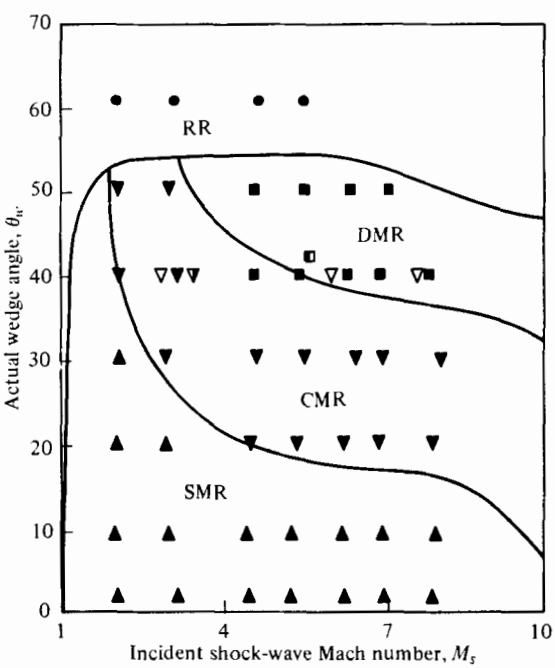

FIGURE 12. Experimental verification of analysis of oblique shock-wave reflexion in (M_s, θ_w) plane for monatomic gases. Lines are for imperfect argon, $P_0 = 15$ Torr, $T_0 = 300$ °K. Data from: Law (1970), CMR in helium (▽); Law & Glass (1971) CMR in argon (▽), Bazhenova *et al.* (1976) DMR in argon (◧). Present results in argon: ■, DMR; ▼, CMR; ▲, SMR; ●, RR.

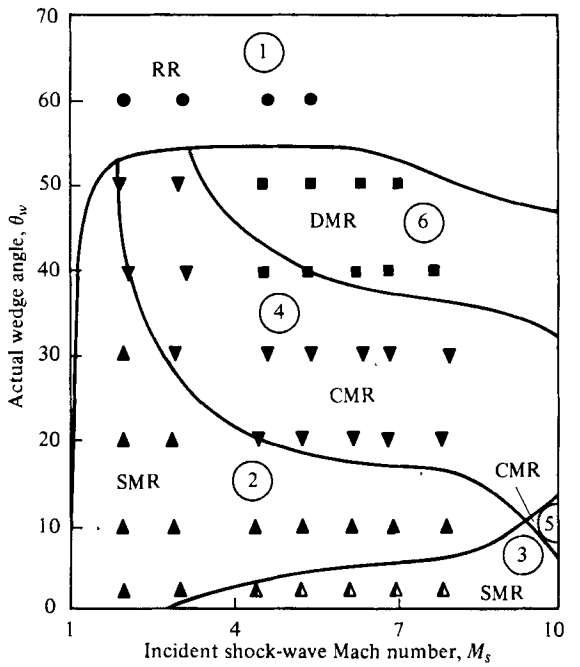

FIGURE 13. Experimental verification of six domains and their transition boundaries of non-stationary oblique shock-wave diffraction. All data points are from the present study. Lines are for imperfect argon, $P_0 = 15$ Torr, $T_0 = 300$ °K. Detached shock wave: ■, DMR; ▼, CMR; ▲, SMR; ●, RR. Attached shock wave: ◭, SMR.

high Mach numbers while in the range $3 \leqslant M_s \leqslant 6$ it is not so good. It should be mentioned here that owing to numerical convergence problems it was not possible to predict χ for these small wedge angles using our analytical version of the graphical method of Law & Glass (1971).

The data of Law & Glass (1971) in helium, Gvozdeva *et al.* (1969), Law & Glass (1971) and the present results in argon are all added to figure 12 (a reproduction of figure 6) in order to check the present analysis of non-stationary oblique shock-wave reflexion in the (M_s, θ_w) plane. Very good agreement with the calculated domains and transition boundaries can be seen. The few experimental points that lie outside their predicted region have already been discussed and accounted for. Therefore it can be concluded that the present analysis of non-stationary reflexions of oblique shock waves in the (M_s, θ_w) plane has been substantiated and verified.

The present data in argon are all shown in figure 13 (a reproduction of figure 8). All the experimental points, except the one at $M_s = 4{\cdot}44$ and $\theta_w = 20°$ (discussed previously), lie inside their predicted domains. Consequently, it can be concluded that the present analysis of non-stationary diffraction of oblique shock waves has been substantiated and verified.

Unfortunately, out of the six different shock-wave diffractions predicted by the present analysis (table 1), only five have been observed experimentally. The remainder, a CMR with an attached shock wave at the wedge corner (region 5, figure 8) was not

tested since its domain starts at $M_s = 9{\cdot}4$, which is beyond the upper limit of incident shock waves we could safely use ($M_s \sim 8$) without damaging the high quality optical windows of the test section. However, in light of the verification of five regions out of the six listed in table 1, and our work in diatomic gases (Ben-Dor & Glass 1979), we believe that we can conclude that the present analysis for the diffraction of oblique shock waves in non-stationary flows is substantiated, and that six different types of shock-wave diffractions exist in the range $1 \leqslant M_s \leqslant 10$.

4. Density fields

Interferograms corresponding to RR, SMR, CMR and DMR in argon are shown in figures 14(*a–d*) (plates 2, 3), respectively. The density field associated with each diffraction in the form of isopycnics (n) are shown in figures 15(*a–d*). The density distribution along the wedge surface and the shock-tube wall in its vicinity are given in figures 16(*a–d*). In the following, a general discussion is given about each diffraction as well as their similarities and differences.

The density field was deduced from the interferograms using a very accurate, semi-computerized method that was developed recently at UTIAS (Ben-Dor, Whitten & Glass 1979). It requires the transformation of the location of fringes into digital form with respect to a chosen reference point. The same physical point is chosen as a reference point for all interferograms (a flow and a no-flow interferogram for each wavelength) for each experiment and is used as an origin. Each fringe can then be thought of as a locus of (x, y) points, i.e. a line having a constant value of fringe number (interference order). With all four interferograms of one experiment digitized in this fashion, with respect to the same reference point, the actual fringe shift, i.e. change in the interference order at any (x, y) co-ordinate, can be easily determined. The interferograms were enlarged to about four times their actual size in order to make the entire digitizing procedure much easier and more accurate. Once the interferograms were digitized, the complete process of analysing the interferograms was done using an IBM 1130 computer (for details see Ben-Dor *et al.* 1979).

The density field corresponding to a RR is shown in figure 15(*a*). A uniform density area can be seen behind the reflexion point P and the straight portion of the reflected shock wave R. The density distribution along the wedge for this RR is shown in figure 16(*a*). The uniform region behind the reflected shock wave is clearly seen. It is terminated by an expansion wave (sound pulses) generated by the wedge corner. Consequently, isopycnic $n = 4$ (figure 15*a*) indicates the upstream distance to which the presence of the wedge corner is felt.

The density field of the SMR shown in figure 15(*b*) indicates that a weak expansion wave originates from the reflected shock wave R near the triple point T (figure 15*b*). The strength of this expansion wave in terms of the density ratio across it is 0·969 (3·560/3·675). This is similar to the results we have recently presented on diatomic gases (Ben-Dor & Glass 1979). The density distribution for this case (figure 16*b*) indicates that the flow passing through the Mach stem is being further compressed from e to d. At the location where the slipstream disappears into the boundary layer a sharp density jump (d–d) is clearly seen.

The density field of a CMR is shown in figure 15(*c*). Unlike the foregoing case of a

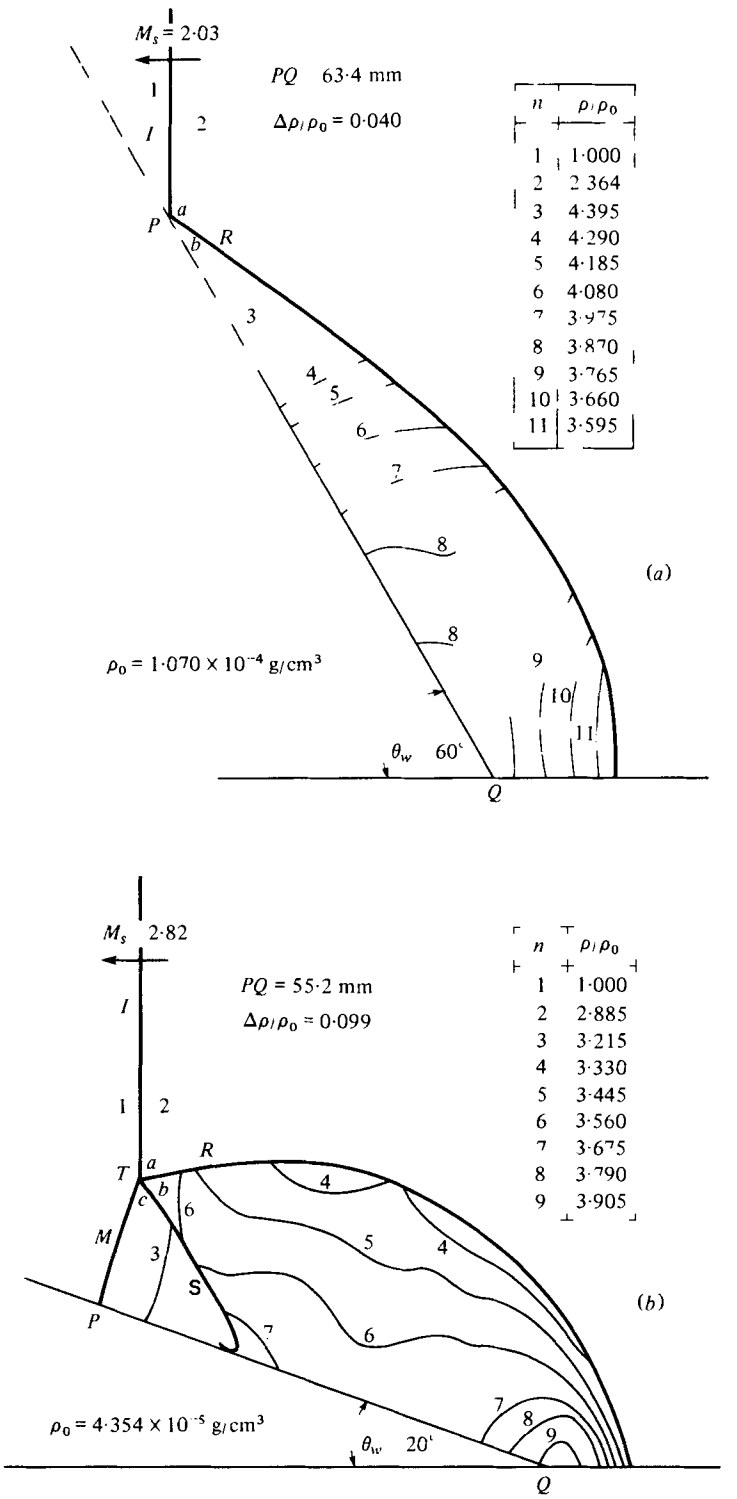

FIGURE 15. For legend see facing page.

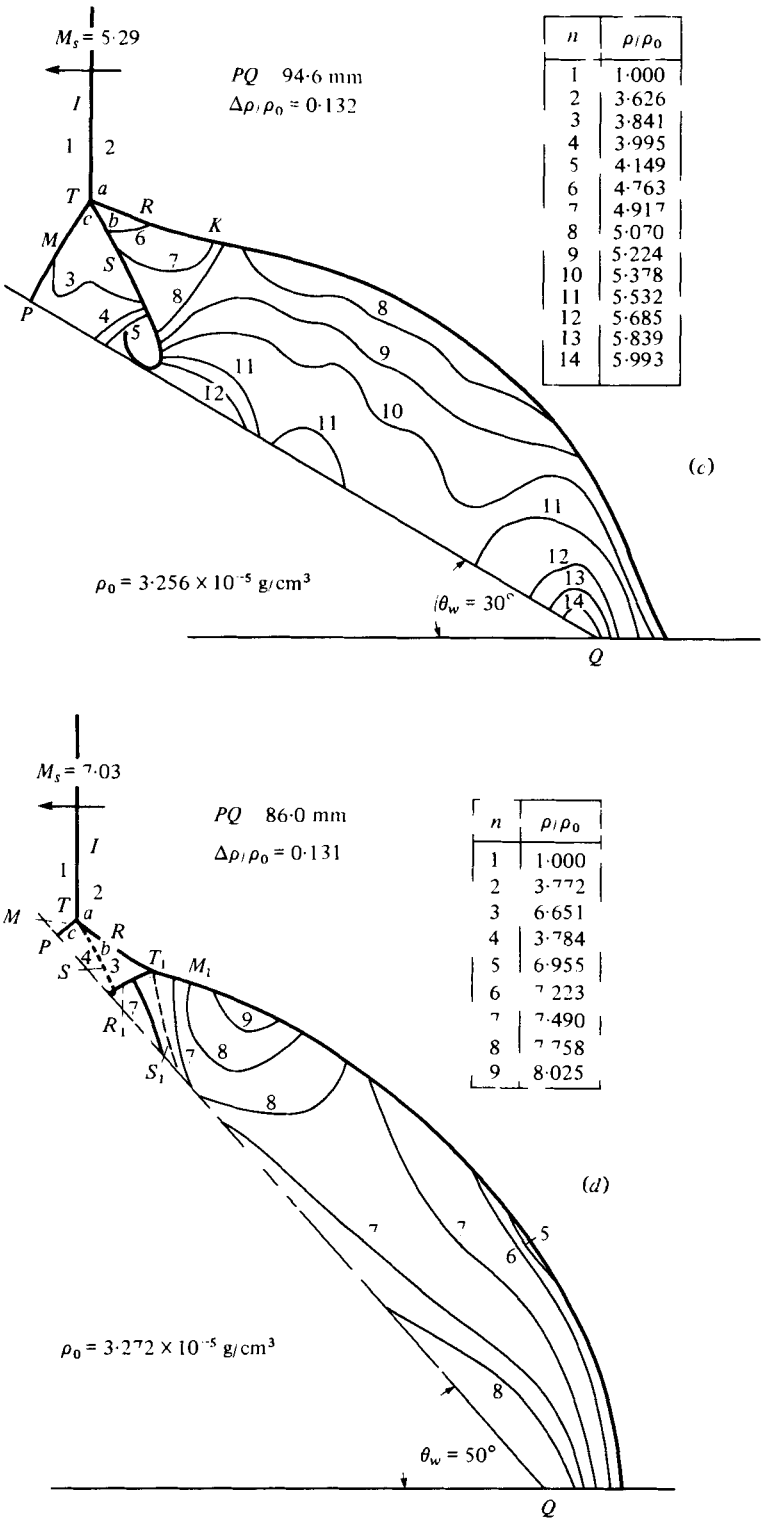

n	ρ/ρ_0
1	1·000
2	3·626
3	3·841
4	3·995
5	4·149
6	4·763
7	4·917
8	5·070
9	5·224
10	5·378
11	5·532
12	5·685
13	5·839
14	5·993

n	ρ/ρ_0
1	1·000
2	3·772
3	6·651
4	3·784
5	6·955
6	7·223
7	7·490
8	7·758
9	8·025

FIGURE 15. Actual flow isopycnics corresponding to the four interferograms shown in figure 14. Calculated densities (ρ/ρ_0) are: (*a*) *a*, 2·314; *b*, 4·329; (*b*) *a*, 2·905; *b*, 3·467; *c*, 3·118; (*c*) *a*, 3·612; *b*, 4·826; *c*, 3·754; (*d*) *a*, 3·771; *b*, 6·522; *c*, 3·909.

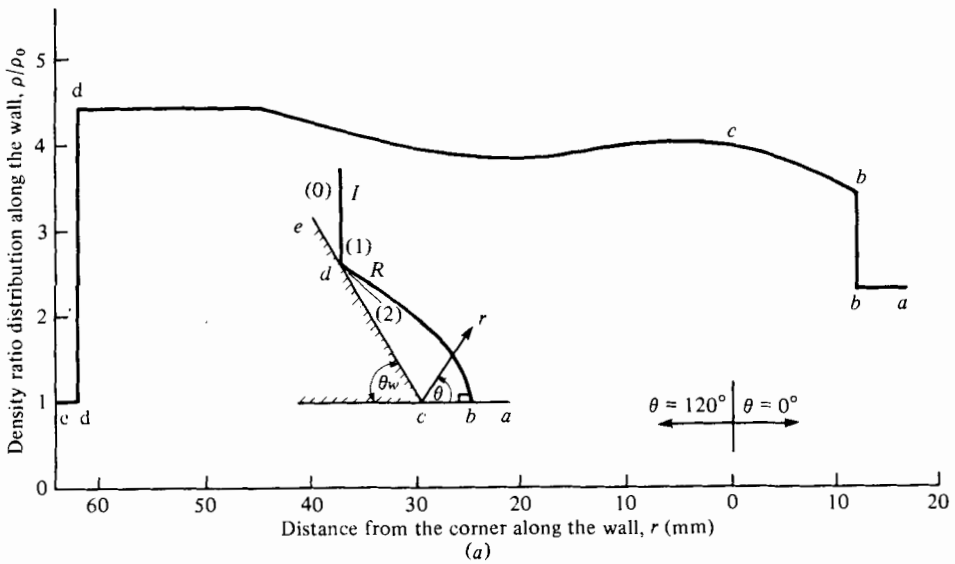

FIGURE 16. For legend see facing page.

SMR where the converging isopycnics at the reflected shock wave R indicated the existence of an expansion wave, here they correspond to a weak compression wave (follow the isopycnic number). The density ratio across this compression wave is 1·031. This compression wave emanates from the kink K in the reflected shock wave. The flow passing through the Mach stem is further compressed on the way towards the place where the slipstream curls back. Unlike the foregoing case of a SMR, here a smooth density change is seen at point d (figure 16c). This probably arises from the slipstream as it curls back far away from the wall, causing the expected discontinuity

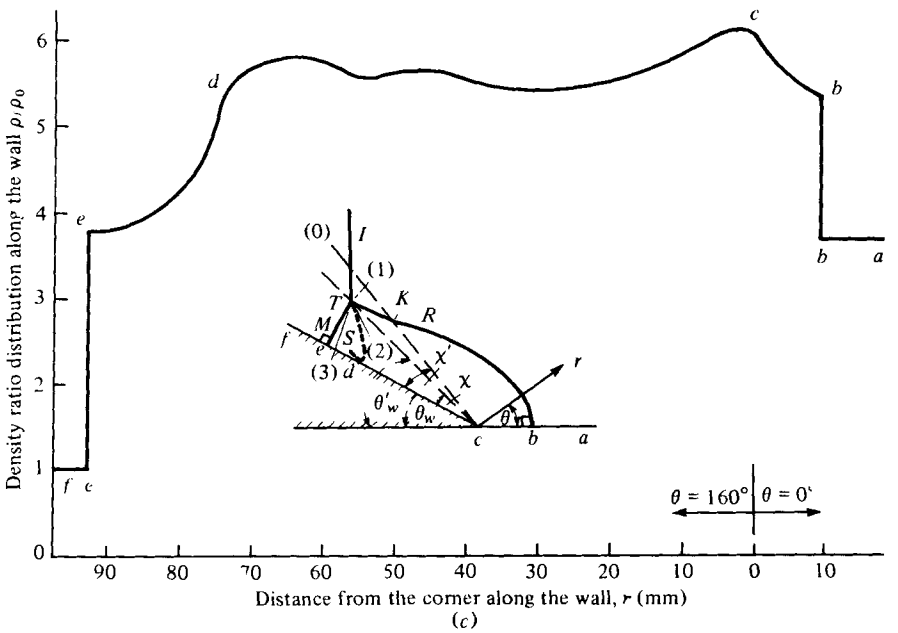

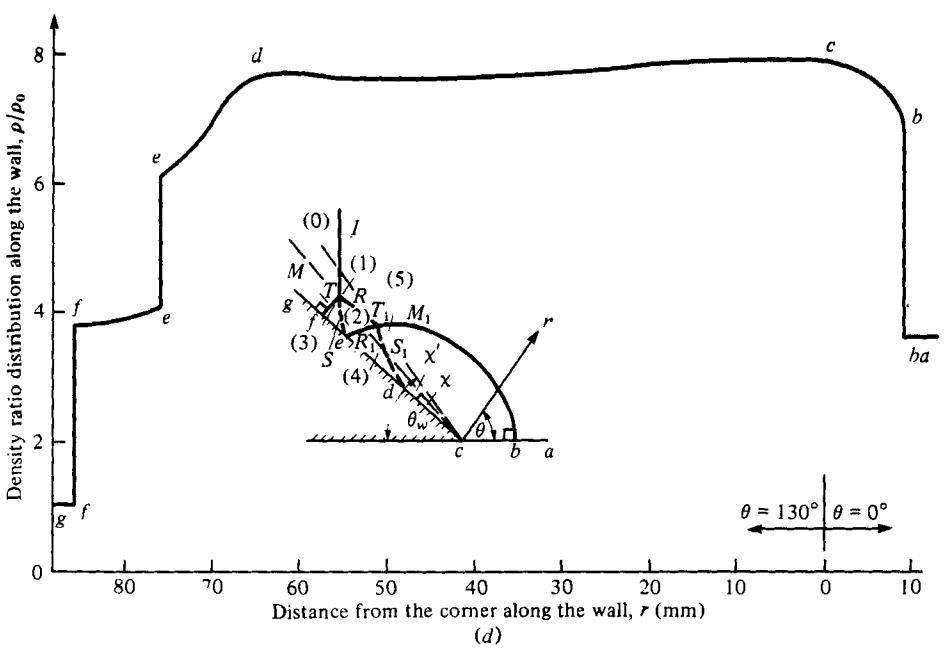

FIGURE 16. Interferometric density-ratio distributions along the wedge surface and the shock-tube wall of the four oblique shock-wave reflexions shown in figure 14 (with identical initial conditions).

near the wall to smear out. The difference between the two slipstreams of these cases are clearly seen in the corresponding interferograms (figures 14*b*, *c*).

The density field of a DMR is shown in figure 15(*d*). The second slipstream of this DMR is not seen in figure 14(*d*), as the density change across it was not large enough to cause a visible fringe shift. However, in figure 15(*d*), two fringes originating from both sides of the second triple point T_1 have the same value ($n = 7$). Consequently, they form a 'corridor' for the second slipstream to exist, as shown schematically by the dashed line.

Although the density fields associated with the various shock-wave diffractions differ greatly from each other, they do have some similarities. In all four cases which correspond to a flow deflexion through a detached shock wave, similar density fields can be seen between the detached shock wave and the wedge corner (figures 15*a–d*). After the density jump (*b–b*) across the detached shock-wave (figures 16*a–d*) the flow is further compressed (*b–c*) on its way towards the wedge corner, where it stagnates. From there on, the density drops gradually before it starts to increase again towards the region affected by the reflexion process. As mentioned above, the flow passing through a Mach stem of a SMR, CMR and DMR is further compressed on its way towards the place where the slipstream disappears into the boundary layer (figures 16*b–d*).

As mentioned earlier, in the foregoing four different types of shock-wave diffraction, the shock-induced flow deflected over the corner was through a detached shock wave. Unfortunately, the flow field associated with deflexion through attached shock waves could not be obtained for the following reasons. The CMR with an attached shock wave (region 5, figure 8) starts at $M_s = 9{\cdot}4$, which is beyond the upper limit of incident shock waves we could safely use ($M_s \leqslant 8$) without damaging the high quality optical windows of the test section. The domain of a SMR with an attached shock wave starts at $M_s = 2{\cdot}758$; however, it involves very small wedge angles ($\theta_w < 10°$). The wedge angle we have used in that region was $\theta_w = 2°$. Unfortunately, the tip of our model for a small wedge angle was not sharp, and an ideally attached shock wave was not obtained.

The density field at any point (x, y) can be calculated either by interpolating between or extrapolating beyond the vicinity of that point. However, since the density difference between the isopycnics is small, any region between the isopycnics can be assumed to have a uniform average density. A region where the change in the density was not sufficiently large to obtain isopycnics within the limits of accuracy can be assumed to be uniform with the indicated density number. For example, region $n = 3$ that is bounded by R, R_1 and S in figure 15(*d*) is uniform with $\rho = 6{\cdot}651\rho_0$. Each fringe shift could be measured to an accuracy of 0·05 to 0·1 of a fringe. Consequently, the relative error in the measured density is given in each figure by $\Delta\rho/\rho_0$, which is fixed for a particular interferogram. It can be as high as 13·2% for $\rho_0 = 0{\cdot}3256 \times 10^{-4}$ g/cm^3 (figure 15*c*) and as low as 4% for $\rho_0 = 0{\cdot}1064 \times 10^{-3}$ g/cm^3 (figure 15*a*). Referring the error to ρ_0 is a severe test. The relative error could be reduced by using ρ_1, which is also well known. The position in the (x, y) plane of any point of a given isopycnic is known to ± 1 mm.

The major importance of these data lies in the fact that argon behaves as a perfect gas in this range of incident shock-waves ($M_s < 7$). Consequently, unlike our data for

nitrogen (Ben-Dor & Glass 1979) where all the analysed diffractions were in a range where vibrational excitation was significant ($M_s > 2$ for nitrogen), the density fields and distributions shown in figures 15 and 16, respectively, are free from real-gas effects. Therefore, our data form a very accurate and comprehensive base for comparison with inviscid numerical analyses, as the refraction errors due to sidewall boundary layers are negligible (Glass & Liu 1978; Liu, Whitten & Glass 1978). Consequently, the interferometric isopycnics of the flow can be used now and in the future as a check in the development of computational methods for non-stationary oblique shock-wave reflexions.

5. Discussions and conclusions

The above comparisons of our analysis and experiments from different sources verify the domains and boundaries of non-stationary reflexion of oblique shock waves in the (M_s, θ'_w) and (M_s, θ_w) planes, as well as the non-stationary diffraction of oblique shock waves in the (M_s, θ_w) plane. It was shown that six regions exist for a monatomic gas, consisting of the basic four types of regular, single-Mach, complex-Mach and double-Mach reflexions. The transition boundaries depend on the incident shock-wave Mach number M_s and the compression wedge angle θ_w for a perfect gas and additionally on the initial temperature T_0 and pressure P_0 for an imperfect gas. Unlike steady flows in wind tunnels, where only regular and single-Mach reflexions are possible, non-stationary flows in shock tubes give rise to two additional complex- and double-Mach reflexions. The fundamental reason lies in the fact that non-stationary shock-wave diffractions consist of two elements. One is the shock-wave reflexion process at the wedge surface and the other is the deflexion of the flow over the wedge induced by the moving shock wave. This flow can be subsonic, transonic or low supersonic. The deflexion of the supersonic flow over the wedge also produces attached or detached bow waves.

The analysis was substantiated by nearly 50 interferometric experiments conducted in the UTIAS 10 cm × 18 cm hypervelocity shock tube during the present study as well as those from Law & Glass (1971) and other sources. The results fall into the six predicted domains separated by their transition boundaries. A new method for the prediction of χ at very low wedge angles was introduced. This method complements the method of Law & Glass (1971), which was found to be good only in the range $5° \leqslant \theta_w \leqslant 45°$. Although these two methods predict χ quite well, a more accurate analytical method is needed. The method for predicting the second triple-point trajectory angle χ' of a DMR also needs further improvement.

The very comprehensive (and first of its kind for monatomic gases) isopycnic data complement our previous work in diatomic gases (Ben-Dor & Glass 1979). The results provide an important base for testing available and future computational codes describing such complex flows of perfect gases. So far really reliable numerical methods in this area have not been developed to date, despite several attempts in the U.S.S.R. and U.S.A. (Ben-Dor & Glass 1978). Undoubtedly, these methods will be forthcoming in the future which will be able to deal with all four types (RR, SMR, CMR, DMR) of oblique shock-wave reflexions.

Finally, it may be concluded that our analyses and numerous experiments in

monatomic and diatomic gases have finally brought order and clarity into a very complex gas-dynamic area which has occupied many researchers over the world for over three decades.

The financial assistance received from the U.S. Air Force under Grant No. AF-AFOSR-77-3303 and from the National Research Council of Canada is gratefully acknowledged.

REFERENCES

AULD, D. J. & BIRD, G. A. 1976 *A.I.A.A. Paper* no. 76-322.

BAZHENOVA, T. V., FOKEEV, V. P. & GOVZDEVA, L. G. 1976 *Acta Astronautica* **3**, 131–140.

BEN-DOR, G. 1978*a* *UTIAS Rep.* no. 232.

BEN-DOR, G. 1978*b* *UTIAS Rep.* no. 237.

BEN-DOR, G. & GLASS, I. I. 1978 *A.I.A.A. J.* **16**, 1146–1153.

BEN-DOR, G. & GLASS, I. I. 1979 *J. Fluid Mech.* **92**, 459–496.

BEN-DOR, G., WHITTEN, B. T. & GLASS, I. I. 1979 *Int. J. Heat Fluid Flow* **1** (2), 77–91.

BLEAKNEY, W. & TAUB, A. H. 1949 *Rev. Mod. Phys.* **21**, 584–605.

FLETCHER, C. H. 1951 *Dept. Phys., Princeton Univ. Tech. Rep.* II-4.

GLASS, I. I. & LIU, W. S. 1978 *J. Fluid Mech.* **84**, 55–77.

GVOZDEVA, L. G., BAZHENOVA, T. V., PREDVODITELEVA, O. A. & FOKEEV, V. P. 1969 *Astronautica Acta* **14**, 503–508.

HENDERSON, L. F. 1964 *Aero. Quart.* **15**, 181–197.

HENDERSON, L. F. & LOZZI, A. 1975 *J. Fluid Mech.* **68**, 139–155.

HORNUNG, H. G., OERTEL, H., JR. & SANDEMAN, R. J. 1979 *J. Fluid Mech.* **90**, 541–560.

JONES, D. A., MARTIN, P. M. & THORNHILL, C. K. 1951 *Proc. Roy. Soc.* A **205**, 238–248.

KAWAMURA, R. & SAITO, H. 1956 *J. Phys. Soc. Japan* **11**, 584–592.

LAW, C. K. 1970 *UTIAS Tech. Note* no. 150.

LAW, C. K. & GLASS, I. I. 1971 *CASI Trans.* **4**, 2–12.

LIU, W. S., WHITTEN, B. T. & GLASS, I. I. 1979 *J. Fluid Mech.* **87**, 609–640.

MACH, E. 1878 *Akad. Wiss. Wien* **77**, II, 1228.

MOLDER, S. 1960 *UTIAS Tech. Note* no. 38.

MOLDER, S. 1979 *CASI Trans.* **25**, 45–49.

NEUMANN, J. VON 1943 *Dept. Navy, Bureau of Ordnance, Re.* 2c, *Washington, D.C. Explosive Res. Rep.* no. 12.

NEUMANN, J. VON 1945 *Dept. Navy, Bureau of Ordnance, Washington, D.C. NAVORD Rep.* no. 203–45.

SEEGER, R. J. & POLACHECK, H. 1943 *Dept. Navy, Bureau of Ordnance, Re.* 2c, *Washington, D.C. Explosive Res. Rep.* no. 13.

SMITH, L. G. 1945 *Office Scientific Res. & Development, Washington, D.C. Rep.* no. 4943.

TAUB, A. H. 1947 *Phys. Rev.* **72**, 51–60.

WHITE, D. R. 1951 *Dept. Phys., Princeton Univ. Tech. Rep.* no. II-10.

WHITE, D. R. 1952 *Proc. 2nd Midwestern Conf. Fluid Mech.*

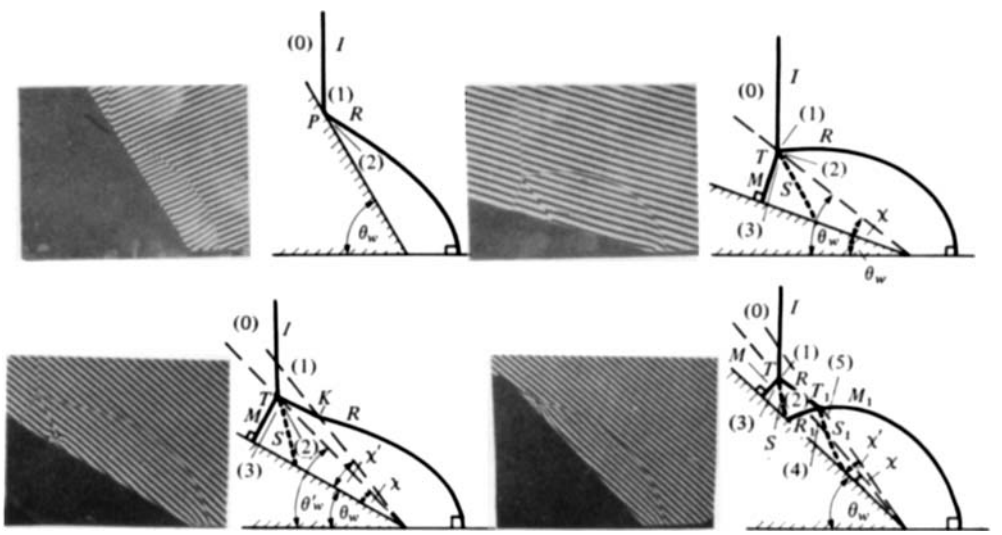

FIGURE 1. Illustration of four possible oblique shock-wave reflexions. (Interferograms are on the left and explanatory sketches on the right.) The interferograms (λ = 6943 Å) were taken with the 23 cm diameter Mach–Zehnder interferometer of the UTIAS 10 cm × 18 cm hypervelocity shock tube in argon at initial pressure $P_0 \approx 15$ Torr and temperature $T_0 \approx 300$ K. I, I_1, incident shock waves; R, R_1, reflected shock waves; M, M_1, Mach stems; S, S_1, slipstreams; T, T_1, triple points; χ, χ', triple-point path angles; K, kink; (0)–(5), thermodynamic states; θ_w, actual wedge angle; θ'_w, effective wedge angle; M_s, shock wave Mach number. (*a*) Regular reflexion (RR), $\theta_w = 60°$, $M_s = 2{\cdot}03$. (*b*) Single-Mach reflexion (SMR), $\theta_w = 20°$, $M_s = 2{\cdot}82$. (*c*) Complex-Mach reflexion (CMR), $\theta_w = 30°$, M 5·29. (*d*) Double-Mach reflexion (DMR), $\theta_w = 50°$, $M_s = 7{\cdot}03$.

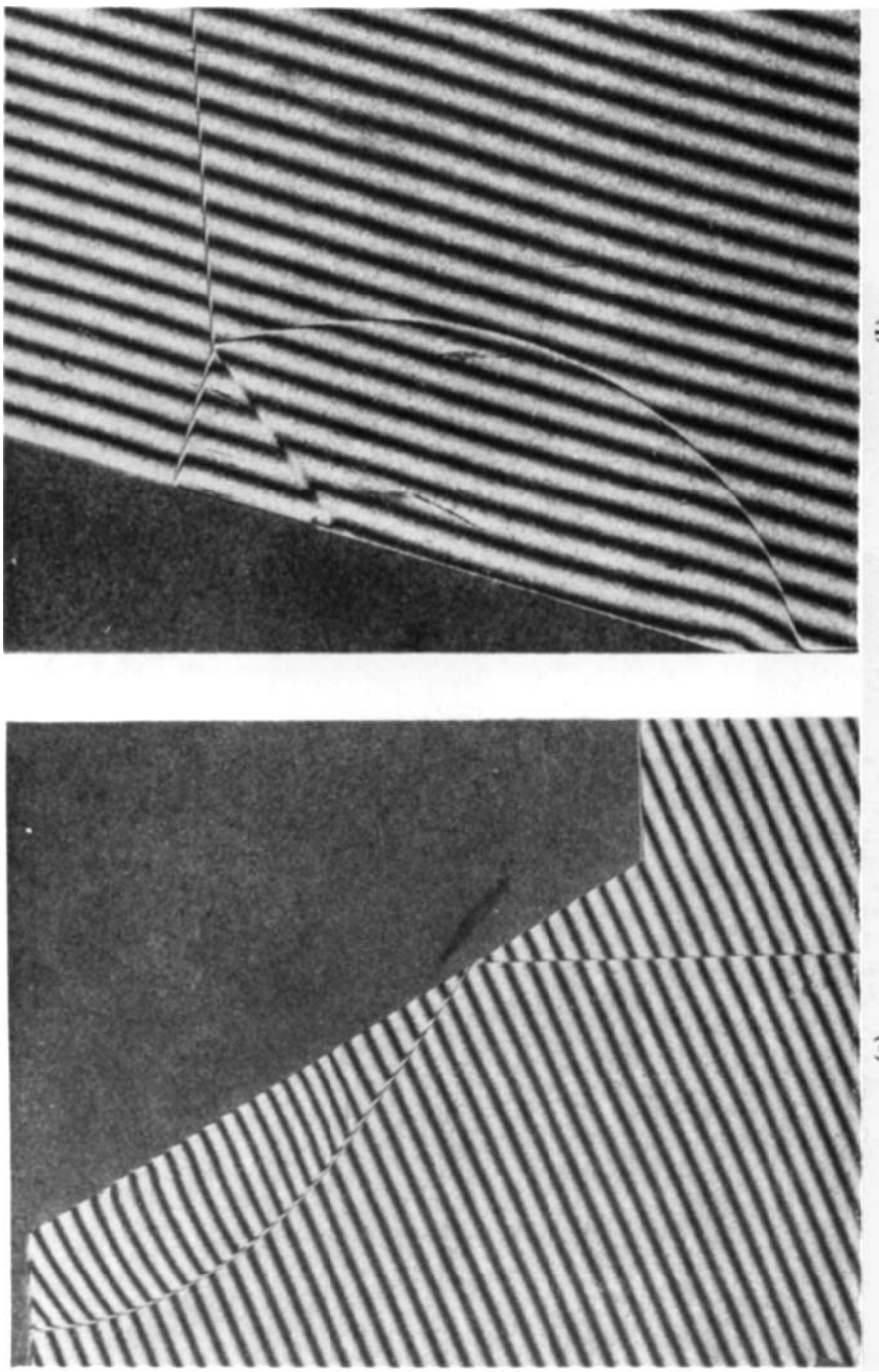

FIGURE 14 (*a*, *b*). For legend see facing page.

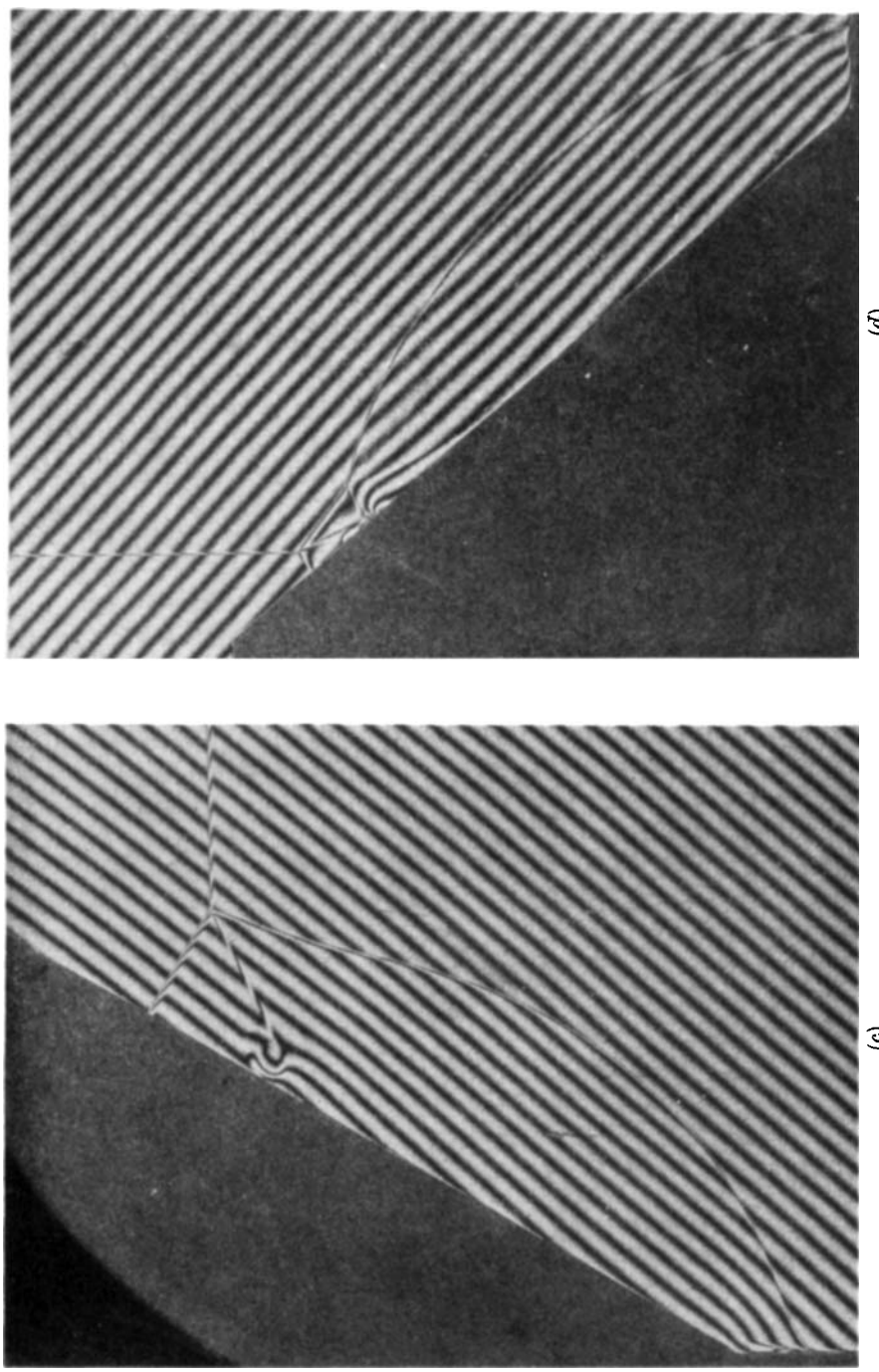

FIGURE 14. Interferograms of four different types of oblique shock-wave reflexions (all with detached shock waves) in argon in non-stationary flows. (*a*)-(*d*) ($\lambda = 6943$ Å) correspond to regions (1), (2), (4) and (6) of figure 8 respectively. (*a*) RR, $M_s = 2{\cdot}03$, $\theta_v = 60^\circ$. (*b*) SMR, $M_s = 2{\cdot}82$, $\theta_w = 20^\circ$. (*c*) CMR, $M_s = 5{\cdot}29$, $\theta_w = 30^\circ$. (*d*) DMR, $M = 7{\cdot}03$, $\theta_w = 50^\circ$.